Mathematical Biosciences and Engineering

https://www.aimspress.com/journal/mbe

MBE, 22(11): 2807–2825.
DOI: 10.3934/mbe.2025103
Received: 26 June 2025
Revised: 31 July 2025
Accepted: 07 August 2025
Published: 12 September 2025

Research article

Mathematical modeling of the immune response mediated by human T-helper lymphocytes in viral diseases

Ledyz Cuesta-Herrera[1,*], Luis Pastenes[2], Fernando Córdova-Lepe[1] and Ariel D. Arencibia[3]

[1] Departamento de Matemática, Física y Estadística, Universidad Católica del Maule, Talca 3480112, Chile

[2] Departamento de Biología y Química, Universidad Católica del Maule, Talca 3480112, Chile

[3] Centro de Biotecnología de los Recursos Naturales (CENBio), Universidad Católica del Maule, Talca 3480112, Chile

* **Correspondence:** Email: lcuesta@ucm.cl.

Abstract: Adaptive immunity, performed by T and B lymphocytes, seeks total virus elimination through specific recognition of viral antigens. It has been shown that innate or adaptive immune response regulation variations are associated with an excessive immune response, leading to tissue damage with an increased risk of complications and death. This article is a novel contribution focused on models that represent pathogenic interactions with humans. In our case, the objective was to build and analyze a mathematical model for SARS-CoV-2 infection in the human host, including elements of respiratory cell dynamics, viral particles, and immune-responding cells. The methodology developed considered modeling by means of ordinary differential equations, validation by comparing referenced studies, and sensitivity analysis with respect to the variables considered. Finally, a comparison of simulation models was performed, verifying that an increase in viral particles increases the response of some adaptive immune system cells in the human host.

Keywords: T Helper cells; coronavirus; immune system; mathematical model

1. Introduction

Mathematical models have been standardized to understand the dynamics of viral infections at the cellular level [1]. Most models fall into the limited target cell model category with some variations. In the case of viral infections, initial cellular interaction models include: 1) uninfected susceptible target cells, corresponding to epithelial cells in the present work, located in the airways of the nasal, tracheal, bronchial, and alveolar mucosa [2–4]; 2) virus-infected cells, where the virus replicates and is subsequently released if cell lysis occurs [5–7].

Understanding the immune response to viral diseases infection is essential as the number of infected patients increases. Currently, there is a lack of clarity about the biological and genetic factors responsible for the severity of the disease, leading to little knowledge about post-infection immunity [8].

The process of viral RNA replication, producing copies of messenger RNA (mRNA), begins when the genetic material of RNA viruses, such as influenza virus, respiratory syncytial virus (RSV), rhinovirus, and coronaviruses including SARS-CoV-2, enters the host cell, serving as templates for the generation of virions that will be used for the formation of new viral particles. After a period of time, the infected cell loses its ability to maintain physical integrity and undergoes cell lysis, leading to the release of new virions [9–11].

It has been suggested that partially neutralizing antibodies and $TCD4+$ and $TCD8+$ lymphocyte responses may be associated with the severity of viral diseases, with age being an important risk factor [11, 12].

Reviews of humoral and cellular immunity to SARS-CoV-2 in humans have been conducted, providing background to understand the dynamics of B and C cell responses, as well as information on the duration of immunity to viral infection, which could lead to the development of new treatments [13–15].

Currently, a large number of papers have formulated mathematical models considering contagion dynamics between organisms; however, a significantly smaller number of investigations have dealt with the spread of the virus within the host [16–18]. These models aim to predict the rate of viral propagation with varying degrees of complexity in susceptible cells [19, 20], which, in the case of SARS-CoV-2 infection, correspond to the cells of the respiratory epithelium, and represent the amount of infecting virus or viral antigens. Some of these models may also involve components of the cellular or humoral immune response [1].

Mathematical modeling can help anticipate both the behavior of the viral infection and the subsequent immune response in the human host [21]. A key feature of most models is that they exhibit a behavioral threshold at which the number of people infected by the infection will either decline on its own or become epidemic [22–24].

In addition, changes in the behavior of virus propagation between cells, as a result of different therapeutic interventions (e.g., vaccinations) or the occurrence of genetic variations that modify the characteristics of the virus, can be included in the analysis through mathematical modeling [25], which allows different scenarios of infection that currently cannot be addressed by direct experimentation.

This work makes a novel and distinctive contribution to the modeling of the dynamics of viral diseases at the intra-host level. In the mathematical modeling process, we have considered the activation of T-helper lymphocytes (T_h) as a starting point. In this line, the purpose of this work is to build a mathematical model of SARS-CoV-2 viral infection in host cells, involving the effect of components of the immune system response. This model will allow a better understanding of the importance of each component in an efficient and balanced immune response and help determine the changes that lead to a deficient or excessive immune response, with the consequent appearance of health complications.

2. Materials and methods

2.1. Overview of the model

Mathematical models related to viral dynamics in the host generally include the interaction of variables that quantify the number of susceptible cells, infected cells, and pathogenic particles [18, 19, 26], improving the understanding of these interactions and allowing human intervention to moderate their effects [27].

The mathematical approach of this work considers a first model proposed by [28], which shows the interaction between a replicating virus and the host cells through the following system of differential equations:

$$\begin{cases} E' &= \lambda - dE - \kappa EV, \\ I' &= \kappa EV - \alpha I, \\ V' &= \nu I - \mu V, \end{cases} \tag{2.1}$$

where referring to an instant t, $E = E(t)$ is the number of susceptible cells [Cells], $I = I(t)$ is the number of infected cells [Cells] activated by the virus to initiate viral replication, and $V = V(t)$ is the number of free viral particles [$copies/mL$].

To introduce the parameters of System (2.1), we begin by referring to the conceptual model illustrated in Figure 1. In this schematic, free viral particles together with epithelial cells, assuming mass action encounters, produce infected cells at a rate κEV, where κ is the number of epithelial cells that one unit of viral concentration infects per unit of time. Each infected cell increases the concentration of viral particles at a rate ν. Epithelial cells are assumed to be generated at a constant rate λ from a pool of precursor cells.

Epithelial cells, infected cells, and free viral particles decrease at unit rates d, α, and μ, respectively. In addition, the ratio ν/α represents the rate of generation of free viral particles per infected cell, adjusted per unit time.

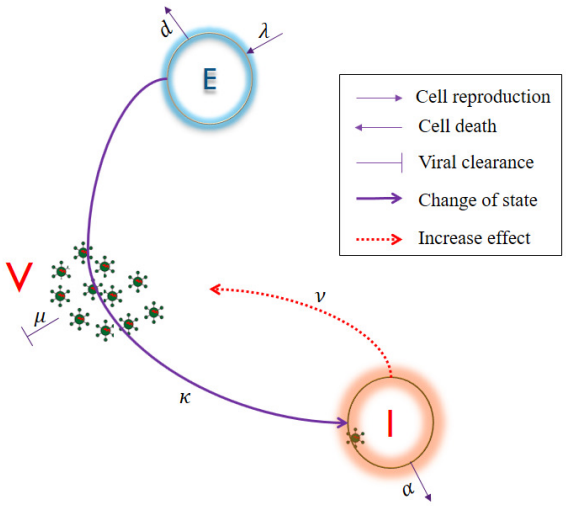

Figure 1. Conceptual model in the absence of immune response associated with the state variables E, V, and I, and System (2.1) parameters. Modified from [28].

Note that without the presence of viral load, we have $E(t) = \lambda/d + (E_0 - \lambda/d)e^{-d(t-t_0)}$, where $E_0 = E(t_0)$. Then $E \to \lambda/d$ if $t \to \infty$, i.e., you would expect to find the system stabilized in epithelial cells.

In order to establish the conditions under which the virus does not spread during $t > 0$ (i.e., after infection time $t = 0$), the reproductive number in the host is defined. The reproductive number for cell models R_0 is defined as the number of newly infected cells that are generated from a first infected cell when the virus is introduced into a population of susceptible cells (epithelial cells) [26].

In this sense, a first infected cell releases viral particles at a rate ν, generating a viral concentration for an average time α^{-1}. These particles can infect susceptible epithelial cells that regenerate at a rate λ and degrade at a rate d, leading to an average epithelial load λ/d. Thus, the expected number of new infected cells is $R_0 = \kappa(\lambda/d)(\nu/\mu)\alpha^{-1}$, which represents the basic viral reproduction number.

In case $R_0 < 1$, it is assumed that the infection is eliminated, i.e., the virus cannot reproduce, resulting in a viral load that tends to zero. Therefore, on average, each virus-infected cell produces, less than one new infected cell. It is then predicted that the infection will disappear from the population or that the virus will be eliminated from the individual, so that the infection cannot spread, and the system returns to the uninfected state [15].

When $R_0 > 1$, the infection progresses, and the virus can invade the susceptible cell population. The magnitude of R_0 is also used to measure the risk of an epidemic or pandemic in an emerging infectious disease [29–31], as it has been important in understanding different viral outbreaks and diseases in the past, such as severe acute respiratory syndrome (SARS) [32–34], new influenza strains [35–37], West Nile virus [38], and others.

The innate immunity mechanisms provide the initial defense against infection and consist of barriers that prevent pathogens from entering the body. If a pathogen (or antigen) crosses these barriers, adaptive immune responses arise and require the activation of T helper lymphocytes (T_h) [39], which respond to the antigen and produce cytokines.

Once the T_h lymphocytes are activated, they secrete cytokines that contribute to the activation of B and cytotoxic T lymphocytes (T_c). They can also activate various phagocytic cells, allowing them to destroy microorganisms more effectively. This type of cell-mediated immune response is particularly important in ridding the host of bacteria, viruses, and protozoa contained in infected host cells [40]. Then, to address the modeling of T_h lymphocyte activation, a base model of activation is proposed, as shown in System (2.2).

$$\begin{cases} E' &= \lambda - dE - \kappa EV, \\ I' &= \kappa EV - \alpha I - \beta T_h I, \\ V' &= \nu I - \mu V - \tau T_h V, \\ T_h' &= b - cT_h + \gamma I T_h, \end{cases} \tag{2.2}$$

where, in addition to the variables defined in (2.1), $T_h = T_h(t)$ are the activated *helper* lymphocytes generated at a constant rate b from a pool of precursor lymphocytes that decrease at a rate c.

In System (2.2), adaptive immunity is induced by specific interactions of T lymphocytes with antigens presented by antigen-presenting cells (APCs). Peptide antigens presented by the major histocompatibility complex (MHC) are exposed to T_h cells [40] at a rate that depends on the amount of I and γ.

T_h lymphocytes act via cytokines to promote other immune reactions. The T_{h_1} lymphocyte response initiates inflammation and immunity by activating macrophages and T_c lymphocytes [40, 41] at a rate of $\beta T_h I$.

The T_{h_2} lymphocyte response stimulates antigen-exposed B lymphocytes to differentiate into antibody-producing plasma cells, which are soluble proteins that interact with specific antigens and provide targets for the action of complement system proteins, resulting in the neutralization and elimination of viral particles [40, 41] at a $\tau T_h V$ rate.

This is shown in the conceptual model in Figure 2.

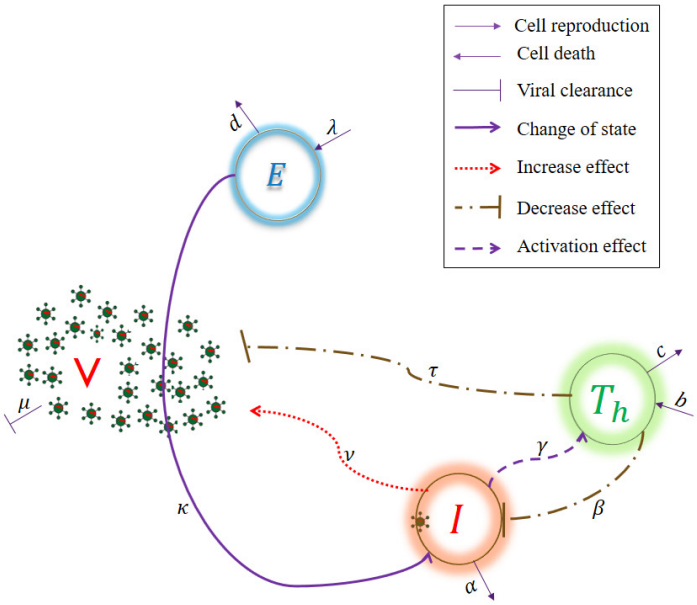

Figure 2. Conceptual model of the presence of immune response associated with System (2.2), complementing Figure 1.

2.2. *Model analysis*

An equilibrium point of steady state variables in time is stable if all trajectories starting in its vicinity remain in that environment; otherwise, the equilibrium point is unstable. Furthermore, an equilibrium is asymptotically stable if it is stable, and all nearby solutions tend in the future toward equilibrium [42].

To preserve the biological sense, the variables of System (2.2) must be non negative, since they represent unit accounting. It must be shown that $E(t) \geq 0, I(t) \geq 0, V(t) \geq 0$ and $T_h \geq 0$, for all $t \geq 0$. Assuming non negativity, then, the states are in the positively invariant region $\Omega = \mathbb{R}^4_+$, and generation and elimination are defined as a function of the population $N = E + I$ with $\lambda = Ed + I\alpha$, where $d = \alpha$. Then, $\lambda = (E + I)\alpha$ defining $D = (E + I)\alpha$, we have $\lambda = D$ and $b = T_h c$.

The initial conditions of System (2.2) are assumed to be a healthy steady state before the infection time $t = 0$, i.e., $V(t) = 0, I(t) = 0, T_h(t) = T_{h_0}$, and $E(t) = E_0$, for all $t < 0$. At time $t = 0$, a small number of virions enter the host organism.

From System (2.2), three equilibrium points are obtained:

1) The infection-free equilibrium denoted by x_0, which represents the state reached in the absence

of viral infection, i.e., it shows the values toward which cell populations tend in the absence of infection ($I = V = 0$), i.e., $x_0 = (E_0, 0, 0, T_{h_0})^t$ where $E_0 = \lambda/d$ and $T_{h_0} = b/c$;

2) The equilibrium with viral infection denoted by x_1, i.e., assuming $T_h = 0$ and $b = 0$, then $x_1 = \left(\frac{\alpha\mu}{\kappa\nu}, \frac{\kappa\lambda\nu - \alpha d\mu}{\alpha\kappa\nu}, \frac{\kappa\lambda\nu - \alpha d\mu}{\alpha\kappa\mu}, 0\right)^t$; and
3) The equilibrium with lymphocyte activation response T_h, denoted by $x_2 = (x_{21}, x_{22}, x_{23}, x_{24})^t$.

The basic reproductive number associated with System (2.2) will be denoted by R_0^*. Importantly, the equilibrium of either viral infection or lymphocyte activation response T_h will not be locally asymptotically stable when $R_0^* < 1$. Consequently, if an individual is at risk of acquiring the disease, but satisfies $R_0^* < 1$, then infection is not established in the organism. The above is developed in Theorems 1 and 2, in whose proofs the classical eigenvalue sign theory, the Routh-Hurwitz criterion, and Descartes' method [42] are used.

Given an initial condition of System (2.2) with $V_0 = V(t_0) > 0$, we say that the virus spreads in the host organism from t_0 if there exists at least one $t^* > t_0$ such that $V(t^*) > V_0$. On the other hand, the virus does not spread if $V(t)$ is strictly decreasing for all $t > t_0$, whether or not the virus reaches a maximum. This is a crucial difference between acute and chronic infection models [19, 26, 27].

The relationship between the reproductive number, R_0^*, at the time of infection and the ability of the virus to spread is established by the following theorem.

Theorem 1. *Let* (2.2)*, defined on* Ω *and with initial time-state condition* $(t_0, (E_0, I_0, V_0, T_{h_0}))$*, with* E_0, V_0*, and* T_{h_0} *positive. Then, if* $R_0^* < 1$*, the virus does not spread from* t_0*. That is, the viral infection-free equilibrium is locally asymptotically stable.*

Remark 1. *Theorem 1 states that if a person is at risk of becoming infected with SARS-CoV-2, but satisfies* $R_0^* < 1$*, then the viral infection is not established in their body, i.e., it cannot spread, and the system returns to the uninfected state.*

Proof. To derive the expression for the reproductive number R_0^*, the next generation matrix method [43] is used in System (2.2).

This system is first ordered so that the infections appear in the first two equations, as shown in the equation:

$$\begin{cases} I'(t) = \kappa EV - \alpha I - \beta T_h I, \\ V'(t) = \nu I - \mu V - \tau T_h V \\ \hline E'(t) = \lambda - dE - \kappa EV, \\ T_h'(t) = b - cT_h + \gamma I T_h. \end{cases} \tag{2.3}$$

Thus, if $X = (I, V, E, T_h)$, we have $X' = \mathcal{F}_+(X) - \mathcal{F}(X)$, with:

$$\mathcal{F}_+ = \begin{pmatrix} \kappa EV \\ 0 \\ 0 \\ 0 \end{pmatrix} \quad \text{and} \quad \mathcal{F} = \begin{pmatrix} \alpha I + \beta T_h I \\ \mu V + \tau T_h V - \nu I \\ dE + \kappa EV - \lambda \\ cT_h - \gamma I T_h - b \end{pmatrix}.$$

The variations of the entries of matrices $\mathcal{F}_+$ and $\mathcal{F}$ are:

$$D\mathcal{F}_+ = \begin{pmatrix} 0 & \kappa E & \kappa V & 0 \\ 0 & 0 & 0 & 0 \\ 0 & 0 & 0 & 0 \\ 0 & 0 & 0 & 0 \end{pmatrix}$$

and

$$D\mathcal{F} = \begin{pmatrix} \alpha + \beta T_h & 0 & 0 & \beta I \\ -\nu & \mu + \tau T_h & 0 & \tau V \\ 0 & \kappa E & d + \kappa V & 0 \\ -\gamma T_h & 0 & 0 & c - \gamma I \end{pmatrix},$$

which, evaluated in x_0, are as follows:

$$D\mathcal{F}_+(x_0) = \begin{pmatrix} 0 & \kappa\lambda/d & 0 & 0 \\ 0 & 0 & 0 & 0 \\ 0 & 0 & 0 & 0 \\ 0 & 0 & 0 & 0 \end{pmatrix}$$

and

$$D\mathcal{F}(x_0) = \begin{pmatrix} \alpha + \beta(b/c) & 0 & 0 & 0 \\ -\nu & \mu + \tau(b/c) & 0 & 0 \\ 0 & \kappa(\lambda/d) & d & 0 \\ -\gamma(b/c) & 0 & 0 & c \end{pmatrix}.$$

Then,

$$\mathcal{F} = \begin{pmatrix} \alpha + \beta(b/c) & 0 \\ -\nu & \mu + \tau(b/c) \end{pmatrix}, \mathcal{F}_+ = \begin{pmatrix} 0 & \kappa\lambda/d \\ 0 & 0 \end{pmatrix} \text{and}$$

$$\mathcal{F}^{-1} = \begin{pmatrix} \frac{c}{\alpha c + b\beta} & 0 \\ \frac{c^2\nu}{\alpha bc\tau + b^2\beta\tau + \alpha c^2\mu + bc\beta\mu} & \frac{c}{b\tau + c\mu} \end{pmatrix},$$

matrix $\mathcal{F}_+\mathcal{F}^{-1}$ then represents the matrix of the next generation. Each entry (i, j) of this matrix represents the expected number of secondary infections in compartment i produced by an infected cell introduced into compartment j. The spectral radius of this matrix ($\rho(\mathcal{F}_+\mathcal{F}^{-1})$), i.e., the modulus or the maximum absolute value of its eigenvalues, defines the reproductive number R_0^*.

For System (2.2), the matrix of the next generation is given by

$$\mathcal{F}_+\mathcal{F}^{-1} = \frac{\kappa\lambda}{d} \begin{pmatrix} \frac{\nu}{\{\alpha + \beta(b/c)\}\{\mu + \tau(b/c)\}} & \frac{1}{\mu + \tau(b/c)} \\ 0 & 0 \end{pmatrix},$$

therefore, the reproductive number R_0^* is given by:

$$R_0^* = \frac{\kappa\lambda\nu/d}{\{\alpha + \beta(b/c)\}\{\mu + \tau(b/c)\}} < R_0, \tag{2.4}$$

because $R_0^* = R_0 \cdot \Lambda$ with

$$\Lambda = \frac{\alpha\mu c}{\{\alpha + \beta(b/c)\}\{\mu + \tau(b/c)\}} < 1. \tag{2.5}$$

Note that, compared to the base model of System (2.1), one has $R_0^* < R_0$, since it is easy to prove that $\Lambda < 1$.

To analyze the local stability of the equilibria, we proceed by spectral analysis of the Jacobian matrix $J(x)$, $x = (E, I, V, T_h)$. Let us note that

$$J(x) = \begin{pmatrix} -(d + \kappa V) & 0 & -\kappa E & 0 \\ \kappa V & -(\alpha + \beta T_h) & \kappa E & -\beta I \\ 0 & \nu & -(\mu + \tau T_h) & -\tau V \\ 0 & \gamma T_h & 0 & \gamma I - c \end{pmatrix}.$$

Then the Jacobian matrix evaluated on x_0 is given as follows:

$$J(x_0) = \begin{pmatrix} -d & 0 & -\kappa\lambda/d & 0 \\ 0 & -\{\alpha + \beta(b/c)\} & \kappa\lambda/d & 0 \\ 0 & \nu & -\{\mu + \tau(b/c)\} & 0 \\ 0 & \gamma b/c & 0 & -c \end{pmatrix}. \tag{2.6}$$

In order to find the eigenvalues of $J(x_0)$, we have that $J(x_0) - z \cdot I_4$ equals to

$$\begin{pmatrix} -(d + z) & 0 & -J_{13} & 0 \\ 0 & -(J_{22} + z) & J_{23} & 0 \\ 0 & J_{32} & -(J_{33} + z) & 0 \\ 0 & J_{42} & 0 & -(c + z) \end{pmatrix},$$

where $J_{13} = \kappa\lambda/d$, $J_{22} = \alpha + \beta(b/c)$, $J_{23} = J_{13}$, $J_{32} = \nu$, $J_{33} = \mu + \tau(b/c)$ y $J_{42} = \gamma b/c$. Note their positivity.

Then, the characteristic polynomial of $J(x_0)$ defined by $P(z) = det(J(x_0) - z \cdot I_4)$ is:

$$P(z) = (d + z)(c + z)[(J_{22} + z)(J_{33} + z) - J_{23}J_{32}].$$

Thus, the eigenvalues of $J(x_0)$ are: $z_1 = -d, z_2 = -c$ and the roots of the quadratic polynomial are $Q(z) := z^2 - T\,z + D$, where

$$T = -(J_{22} + J_{33}) \quad \text{and} \quad D = J_{22}J_{33} - J_{23}J_{32}.$$

Let us note that the roots of $Q(z)$ are real since its discriminant $T^2 - 4D$, equal to $[J_{22} - J_{33}]^2 + 4J_{23}J_{32}$, is a positive number. These roots will be negative if $D > 0$. That is, $J_{22}J_{33} > J_{23}J_{32}$. In terms of the original parameters, $\{\alpha + \beta(b/c)\}\{\mu + \tau(b/c)\} > \kappa\lambda\nu/d$, which is equivalent to $R_0^* < 1$. Then, if this is the case, it is verified that the viral infection-free equilibrium, x_0, is locally asymptotically stable.

□

Theorem 2. *Given System* (2.2)*, defined in the positively invariant region* Ω *at the onset of infection, i.e.,* $E(0) = E_0 > 0, I(0) = 0, V(0) = V_0 > 0$ *and* $T_h(0) = T_{h_0} > 0$*. Then, a sufficient condition for the virus to spread is given by* $R_0^* > 1$*, which indicates that the equilibrium with viral infection is locally asymptotically stable if and only if* $R_0^* > 1$.

Remark 2. *Theorem 2 states that if a person is at risk of SARS-CoV-2 infection, and satisfies $R_0^* > 1$, then viral infection is established in their body. Therefore, viral infection progresses and SARS-CoV-2 can invade the epithelial cell population in the following two scenarios: 1) without activating the T_h lymphocyte response; 2) by activating the T_h lymphocyte response.*

Proof. To analyze the stability of the equilibrium with viral infection and without T_h lymphocyte activation, the Jacobian matrix evaluated in x_1 is given by matrix (2.7).

$$J(x_1) = \begin{pmatrix} -\frac{\kappa\lambda\nu}{\alpha\mu} & 0 & \frac{\alpha\mu}{\nu} & 0 \\ \frac{\kappa\lambda\nu}{\alpha\mu} - d & -\alpha & \frac{\alpha\mu}{\nu} & \frac{\beta d\mu}{\kappa\nu} - \frac{\beta\lambda}{\alpha} \\ 0 & \nu & -\mu & \frac{dt}{\kappa} - \frac{\lambda\nu t}{\alpha\mu} \\ 0 & 0 & 0 & \frac{\gamma\lambda}{\alpha} - c - \frac{\gamma d\mu}{\kappa\nu} \end{pmatrix}, \tag{2.7}$$

Remark: If $T_h = 0 \quad \forall t$ then $b = 0$, thus in Eq (2.4), one has

$$R_0^* = \frac{\kappa\lambda\nu}{d\mu\alpha} = R_0.$$

Assuming that

$$R_0^* = \frac{\kappa\lambda\nu}{d\mu\alpha} > 1,$$

if and only if

$$\kappa\lambda\nu - d\alpha\mu > 0,$$

on the other hand, in terms of R_0^*, matrix (2.7) is rewritten as shown in matrix (2.8)

$$J(x_1) = \begin{pmatrix} -dR_0^* & 0 & \frac{\alpha\mu}{\nu} & 0 \\ d\left(R_0^* - 1\right) & -\alpha & \frac{\alpha\mu}{\nu} & -\frac{\beta\lambda\left(R_0^* - 1\right)}{\alpha R_0^*} \\ 0 & \nu & -\mu & \frac{d\left(t - R_0^*\right)}{\kappa} \\ 0 & 0 & 0 & \frac{\gamma\lambda}{\alpha} - c - \frac{\gamma\lambda}{\alpha R_0^*} \end{pmatrix}, \tag{2.8}$$

whose characteristic polynomial is $Q(z) = Q_1(z) \cdot Q_2(z)$, with:

$$Q_1(z) = -z^3 - z^2(\alpha + dR_0^* + \mu) - zdR_0^*(\alpha + \mu) + d\alpha\mu(R_0^* - 1)$$

and

$$Q_2(z) = -z + \frac{\gamma\lambda}{\alpha}\left(1 - \frac{1}{R_0^*}\right) - c.$$

The eigenvalues of matrix (2.8) are $z_1 = \{\gamma\lambda/\alpha\}(R_0^* - 1)/R_0^* - c$, taking into account that the condition of eigenvalue is that

$$z_1 = \gamma\frac{\lambda}{\alpha}\frac{(\kappa\lambda\nu - \alpha d\mu)}{\kappa\lambda\nu} - c < 0,$$

then

$$\kappa\lambda\nu - \alpha d\mu < \frac{c\alpha\kappa\nu}{\gamma}$$

which leads to having

$$\alpha d\mu(R_0^* - 1) < \frac{c\alpha\kappa\nu}{\gamma}$$

which implies that

$$1 - \frac{1}{R_0^*} < \frac{c\alpha}{\gamma\lambda},$$

therefore, $z_1 < 0$ or, equivalently, $1 - \frac{1}{R_0^*} < \frac{c\alpha}{\gamma\lambda}$ and the solutions of Eq (2.9)

$$0 = Q_2(z) = z^3 + Az^2 + Bz + C, \tag{2.9}$$

whose coefficients are:

$A = \alpha + \mu + dR_0^*$, $B = dR_0^*(\alpha + \mu)$ and $C = \alpha d\mu\left(R_0^* - 1\right)$. Since $A > 0$, using the Routh-Hurwitz criterion, the solutions of Eq (2.9) have a negative real part if $AB - C > 0$.

We know that

$$1 < \frac{(\alpha + \mu)^2}{\alpha\mu} \quad \text{therefore}$$
$$1 - \left(\frac{1}{\alpha} + \frac{1}{\mu}\right)(\alpha + \mu) < 0$$

since

$$1 - \left(\frac{1}{\alpha} + \frac{1}{\mu}\right)(\alpha + \mu + dR_0^*) <$$
$$1 - \left(\frac{1}{\alpha} + \frac{1}{\mu}\right)(\alpha + \mu) < 0,$$

it is concluded that $AB - C > 0$, and then

$$AB - C = \alpha d\mu(1 - R_0^*)\left[1 - \left(\frac{1}{\alpha} + \frac{1}{\mu}\right)(\alpha + \mu + dR_0^*)\right].$$

Thus, it is shown that $AB - C > 0$.

Finally, the equilibrium with viral infection, x_1, is locally asymptotically stable if and only if $z_1 < 0$ or, equivalently, $1 - \frac{1}{R_0^*} < \frac{c\alpha}{\gamma\lambda}$.

□

The equilibrium set with T_h lymphocyte activation response, x_2, is of the form $x_2 = (x_{21}, x_{22}, x_{23}, x_{24})^t$, being determined by the following algebraic steps:

1) Solving for I in terms of T_h from the second equation of System (2.2):

$$\gamma I T_h = cT_h - b$$
$$I = \frac{cT_h - b}{\gamma T_h} \tag{2.10}$$

2) Replacing Eq (2.10) in the third equation of System (2.2):

$$0 = \frac{c\nu}{\gamma} - \frac{b\nu}{\gamma T_h} - (\mu + \tau T_h)V. \tag{2.11}$$

3) Isolating E from the first equation of System (2.2):

$$E = \frac{\lambda}{d + \kappa V} \tag{2.12}$$

4) Replacing Eqs (2.10) and (2.12) into the second equation of System (2.2):

$$0 = \frac{\beta(b - cT_h)}{\gamma} + \frac{\alpha(b - cT_h)}{\gamma T_h} + \frac{\kappa\lambda V}{d + \kappa V}. \tag{2.13}$$

5) Isolating V from Eq (2.13)

$$V = \frac{d(\alpha + \beta T_h)(cT_h - b)}{\kappa(\alpha(b - cT_h) + T_h(b\beta + \gamma\lambda - \beta cT_h))}. \tag{2.14}$$

Thus, the equilibrium point x_2 as a function of T_h^* is of the form:

$$\begin{aligned}
x_{21} &= \frac{\alpha(b - cT_h^*) + T_h^*(b\beta + \gamma\lambda - \beta cT_h^*)}{d\gamma T_h^*},\\
x_{22} &= \frac{cT_h^* - b}{\gamma T_h^*},\\
x_{23} &= \frac{d(\alpha + \beta T_h^*)(cT_h^* - b)}{\kappa[\alpha(b - cT_h^*) + T_h^*(b\beta + \gamma\lambda - \beta cT_h^*]},\\
x_{24} &= T_h^*,
\end{aligned}$$

where T_h^* is a solution of:

$$\begin{aligned}
&(cT_h - b)(\alpha b\kappa\nu - \alpha T_h(c\kappa\nu + d\gamma(\mu + T_h\tau))) =\\
&\quad T_h(\beta c\kappa\nu T_h - b\beta\kappa\nu + \gamma(\beta d\mu T_h - \kappa\lambda\nu + \beta d T_h^2\tau))
\end{aligned}$$

which implies that T_h^* is a solution of the polynomial $A_3T_h^3 + A_2T_h^2 + A_1T_h + A_0 = 0$, where the coefficients of the above equation are of the form:

$A_0 = \alpha b\kappa\nu, A_1 = b\beta\kappa\nu - \alpha d\gamma\mu - \alpha c\kappa\nu + \gamma\kappa\lambda\nu, A_2 = -\beta d\gamma\mu - \beta c\kappa\nu - \alpha d\gamma\tau, A_3 = -\beta d\gamma\tau.$

Assuming $T_h^* = b/c$ implies the existence of the viral infection-free equilibrium; however, this is not relevant to the paper since it has been studied before in x_0. Then, $A_3 < 0, A_2 < 0, A_1$ real and $A_0 > 0$, by Descartes' method, there is a unique $T_h^* > 0$ such that $P(T_h^*) = 0$

3. Results and discussion

Some studies suggest that viral load in the lower respiratory tract may peak in the second week after symptom onset [16,27,44]. However, serial measurement of this type of biomarker is complex in practical terms.

Viral load at any given time after diagnosis or detection tends to be similar between asymptomatic and symptomatic patients [45]. However, studies show a tendency for a longer duration of viral shedding in more severe cases and older patients [46–48].

Despite the detection of viral particles in samples from some individuals several weeks after of symptoms onset, these virions are usually not present for more than 8–14 days [49–51].

Authors such as Ejima et al. [52], Gonçalves et al. [13] and Challenger et al. [53] took into account different studies to represent the decrease in viral load after symptoms onset. They found that viral samples testing negative for SARS-CoV-2 are set at 1 $copy\ viral/mL$; also, the mean viral load was calculated for each day, showing that from day 20 onward, more than half of the samples recorded on each of these days were below the limit of detection.

Mathematical modeling of virus dynamics in the host has been carried out using available virological and immunological information from previously studied infections, such as influenza, hepatitis B, HIV infection, and some coronaviruses [19, 27, 52].

However, as the pandemic has unfolded, new virological and immunological studies have added additional information regarding the behavior of the viral infection [54, 55]. In addition, aspects of the immune response that differentiate SARS-CoV-2 infection from other respiratory infections are also being elucidated [8, 56].

Given the above, values of variables and parameters sourced from published literature and summarized in Table 1 were selected to ensure that the resulting viral load aligns with reported values in the literature, particularly in the context of T_h lymphocyte activation. The resulting dynamics under different scenarios are illustrated in Figure 3.

Numerical simulations were performed using R Software version 4.1.2.

Table 1. Estimates of model parameters and variables.

Description / Variables	**Symbol**	**Rank**	**Value System** (2.1)	**Value System** (2.2)	**Reference**
Epithelial cells	E_0	$[1.36 \times 10^4 - 4.81 \times 10^{10}]$	5×10^6	5×10^6	[3,4]
Infected cells	I_0	—	0	0	—
Free viral particles	V_0	$[1 - 6.6 \times 10^8]$	8×10^5	1×10^5	[4,53,56]
Activated T-helper lymphocytes	T_{h_0}	$[4.5 \times 10^6]$	—	5×10^5	—
Epithelial cell generation rate [day^{-1}]	λ	—	25×10^5	5×10^5	—
Epithelial cell death rate [day^{-1}]	d	—	0.5	0.1	—
Probability of epithelial cell infection per viral particle [mL/(copies*day)]	κ	$[0.03 - 13.5] \times 10^{-8}$	0.035×10^{-8}	1×10^{-7}	[3,4,10,53]
Infected cell death rate [day^{-1}]	α	—	0.5	0.1	—
Lysis effect on infected cells [day^{-1}]	β	—	—	1×10^{-7}	—
Replication rate of viral particles [mL/(copies*day*cell)]	ν	$[9.3 - 2 \times 10^3]$	995	995	[4,10,53,57]
Degradation rate of free viral particles [day^{-1}]	μ	[0.39 – 2.51]	0.5	0.5	[4,10,26,53]
Neutralization effect on free viral particles [mL/(copies*day*cell)]	τ	—	—	1×10^{-7}	—
T_h lymphocyte production rate [day^{-1}]	b	—	—	5×10^4	—
T_h lymphocyte death rate [day^{-1}]	c	—	—	0.1	—
Activation effect on T_h lymphocytes [day^{-1}]	γ	—	—	1×10^{-7}	—

3.1. Simulations

Taking into account the parameters in Table 1, System (2.1) shows the spread of infection once the viral load is able to replicate; furthermore, epithelial cells (E) are generated at a rate λ $[day^{-1}]$ and decrease at a rate d $[day^{-1}]$, out of the total cells.

Coronaviruses infect mainly differentiated respiratory epithelial cells [4, 51].

Once cells are productively infected, they release virus at a rate ν $[mL/(copies \times day \times cell)]$ and virus particles are degraded at a rate μ $[day^{-1}]$.

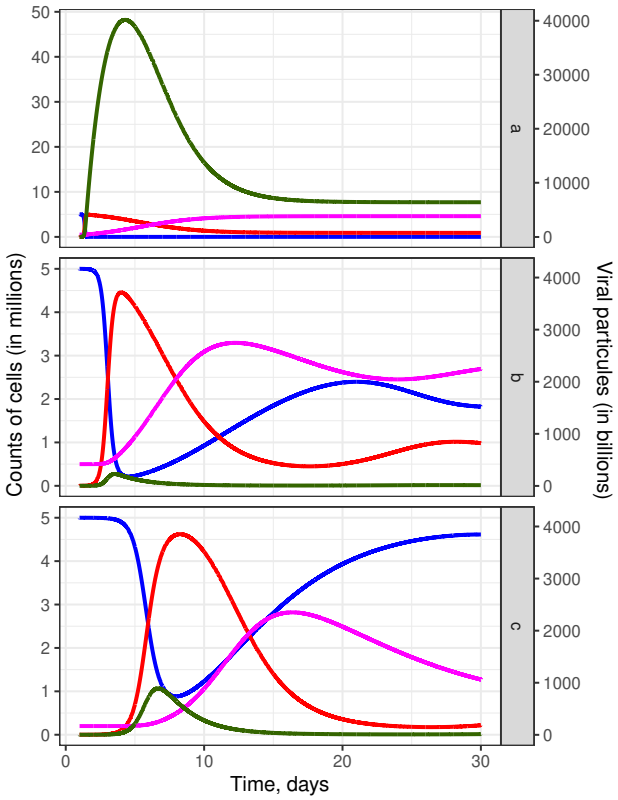

Figure 3. Cell dynamics for a viral infection given by System (2.2) for the parameters in Table 1. Host cells can be in one of the following states: susceptible (E: blue line) or infected (I: red line). Viral particles (V: green line) and T-lymphocyte activation (T_h: magenta line). Figure 3a,b,c is given by System (2.2) with $R_0^* = 6.0303 \times 10^3, R_0^* = 33.0017$, and $R_0^* = 19.8920$, respectively.

Infected cells are eliminated at a rate α $[day^{-1}]$ as a consequence of biochemical and molecular viral effects caused during the viral replication cycle. It must be considered that SARS-CoV-2 virus is an obligate intracellular pathogen, so if there are no susceptible and infected cells, as they eventually die, it will not be able to replicate, leading to a decrease in viral load.

Thus, in a case without adequate immune response or effective therapeutic intervention, progressive cell death of host cells in the respiratory tract can occur, and the viral replication machinery in this model is lost.

In addition, Figure 3a shows the activation of (T_h) lymphocytes, which leads to free virus particles being cleared at a $\tau T_h V$ rate.

Infected cells are eliminated at a rate $\beta T_h I$ as a result of cell lysis and phagocytosis; however, the amount of viral load is so high that although a decrease in infected cells is evident at about day 6, epithelial cells recover until day 30.

Figure 3b shows an increase in the neutralization effect on viral particles, where the decrease in viral load is evidenced approximately on day 10 after infection onset; in turn, the epithelial cells tend to recover, given that the immune response acts in a timely manner once the T_h lymphocytes are

activated, and their effector functions act on the viral particles and infected cells.

Figure 3c shows an increase in the effect of cell lysis and phagocytosis ($\beta = 1.1 \times 10^{-7}$), in the neutralization free viral particles ($\tau = 1 \times 10^{-4}$) and in the proportion of epithelial cell death ($d = 0.2$). In addition, the rate of epithelial cell generation ($\lambda = 1 \times 10^{6}$), the probability of epithelial cell infection per viral particle ($\kappa = 1 \times 10^{-8}$), the initial T_h lymphocytes ($T_{h_0} = 2 \times 10^{5}$), and the rate of T_h lymphocyte generation ($b = 2 \times 10^{4}$) are decreased.

As a consequence, there is evidence of an increase in viral load and a decrease in viral infection at approximately day 15, where epithelial cells tend to recover after infection onset, indicating that although the immune response occurs approximately 5 days later than shown in Figure 3a, it acts on the system in a timely manner through its effector functions on viral particles and infected cells.

4. Conclusions

Despite the increased effect of cells lysis, phagocytosis, and neutralization on free viral particles, T_{h_0} lymphocyte depletion delays viral load degradation and epithelial cells recovery; however, this occurs within a timely range of recovery.

As the effects increase once T_h lymphocytes are activated, it is evident (Figure 3a,b,c) that when the virus is introduced into the susceptible cell population, the number of newly infected cells generated from a first infected cell tends to decrease.

The estimation of parameters for model validation, such as time and lag periods, antibody curves, lymphocyte response monitoring, and cytokine concentrations, allow for better estimation and fine-tuning of the model, leading to a better understanding of the dynamics of viral infection at the cellular level.

This type of cellular immune response is relevant in respiratory diseases caused by viruses such as influenza A, respiratory syncytial virus (RSV), rhinovirus, and coronaviruses including SARS-CoV-2, among others.

Additional elements of the immune response need to be considered in future work, specifically the components of the humoral and cellular response, as well as the regulatory mechanisms of the immune response. This type of cell-mediated immune response is relevant in respiratory diseases caused by viruses such as measles and influenza, among others.

Use of AI tools declaration

The authors declare they have not used Artificial Intelligence (AI) tools in the creation of this article.

Acknowledgments

The authors thanks the Vice-Rectory for Research and Postgraduate Studies, as well as to the PhD Program in Applied Mathematical Modeling at Universidad Católica del Maule, Talca, Chile. This research was funded by Agencia Nacional de Investigación y Desarrollo (ANID) of Chile, Fondecyt Regular, grant number 1231256.

Conflict of interest

The authors declare there is no conflict of interest.

References

1. A. S. Perelson, Modelling viral and immune system dynamics, *Nat. Rev. Immunol.*, **2** (2002), 28–36. https://doi.org/10.1038/nri700
2. R. Blanco-Rodríguez, X. Du, E. Hernández-Vargas, Computational simulations to dissect the cell immune response dynamics for severe and critical cases of SARS-CoV-2 infection, *Comput. Methods Programs Biomed.*, **211** (2021), 106412. https://doi.org/10.1016/j.cmpb.2021.106412
3. S. Wang, Y. Pan, Q. Wang, H. Miao, A. N. Brown, L. Rong, Modeling the viral dynamics of SARS-CoV-2 infection, *Math. Biosci.*, **328** (2020), 108438. https://doi.org/10.1016/j.mbs.2020.108438
4. E. A. Hernandez-Vargas, J. X. Velasco-Hernandez, In-host mathematical modelling of COVID-19 in humans, *Ann. Rev. Control*, **50** (2020), 448–456. https://doi.org/10.1016/j.arcontrol.2020.09.006
5. L. Cuesta-Herrera, L. Pastenes, F. Córdova-Lepe, A. D. Arencibia, H. A. Torres-Mantilla, Cell lysis analysis for respiratory viruses through simulation modeling, *J. Phys. Conf. Ser.*, **2159** (2022), 012002. https://doi.org/10.1088/1742-6596/2159/1/012002
6. Q. Sun, T. Miyoshi, S. Richard, Analysis of COVID-19 in Japan with extended SEIR model and ensemble Kalman filter, *J. Comput. Appl. Math.*, **419** (2023), 114772. https://doi.org/10.1016/j.cam.2022.114772
7. E. Ngondiep, A robust numerical two-level second-order explicit approach to predicting the spread of Covid-2019 pandemic with undetected infectious cases, *J. Comput. Appl. Math.*, **403** (2022), 113852. https://doi.org/10.1016/j.cam.2021.113852
8. S. Q. Du, W. Yuan, Mathematical modeling of interaction between innate and adaptive immune responses in COVID-19 and implications for viral pathogenesis, *J. Med. Virol.*, **92** (2020), 1615–1628. https://doi.org/10.1002/jmv.25866
9. F. C. Schuffeneger, M. Gajardo, M. Freundlich, Eje renina angiotensina, enzima convertidora de angiotensina 2 y Coronavirus, *Rev. Chil. Pediatr.*, **91** (2020). http://dx.doi.org/10.32641/rchped.vi91i3.2548
10. D. A. J. Tyrrell, S. H. Myint, *Coronaviruses*, University of Texas Medical Branch at Galveston, 1996.
11. S. Wang, M. Hao, Z. Pan, J. Lei, X. Zou, Data-driven multi-scale mathematical modeling of SARS-CoV-2 infection reveals heterogeneity among COVID-19 patients, *PLoS Comput. Biol.*, **17** (2021), e1009587. https://doi.org/10.1371/journal.pcbi.1009587
12. P. Vetter, C. S. Eberhardt, B. Meyer, P. A. M. Murillo, G. Torriani, F. Pigny, et al., Daily viral kinetics and innate and adaptive immune response assessment in COVID-19: A case series, *mSphere*, **5** (2020). https://doi.org/10.1128/mSphere.00827-20

13. A. Gonçalves, J. Bertrand, R. Ke, E. Comets, X. De Lamballerie, D. Malvy, et al., Timing of antiviral treatment initiation is critical to reduce SARS-CoV-2 viral load, *CPT: Pharmacometrics Syst. Pharmacol.*, **9** (2020), 509–514. https://doi.org/10.1002/psp4.12543

14. A. Goyal, E. F. Cardozo-Ojeda, J. T. Schiffer, Potency and timing of antiviral therapy as determinants of duration of SARS-CoV-2 shedding and intensity of inflammatory response, *Sci. Adv.*, **6** (2020), eabc7112. https://doi.org/10.1126/sciadv.abc7112

15. L. Cuesta-Herrera, L. Pastenes, A. D. Arencibia, F. Córdova-Lepe, C. Montoya, Dynamics of activation and regulation of the immune response to attack by viral pathogens using mathematical modeling, *Mathematics*, **12** (2024), 2681. https://doi.org/10.3390/math12172681

16. K. A. Pawelek, D. Dor Jr, C. Salmeron, A. handel, within-host models of high and low pathogenic influenza virus infections: The role of macrophages, *PLoS One*, **11** (2016), e0150568. https://doi.org/10.1371/journal.pone.0150568

17. O. O. Okundalaye, W. A. M. Othman, A. S. Oke, Toward an efficient approximate analytical solution for 4-compartment COVID-19 fractional mathematical model, *J. Comput. Appl. Math.*, **416** (2022), 114506. https://doi.org/10.1016/j.cam.2021.113852

18. L. Fan, Z. Qiu, Q. Deng, T. Guo, L. Rong, Modeling SARS-CoV-2 infection dynamics: Insights into viral clearance and immune synergy, *Bull. Math. Biol.*, **87** (2025), 67. https://doi.org/10.1007/s11538-025-01442-0

19. S. M. Ciupe, J. M. Heffernan, In-host modeling, *Infect. Dis. Modell.*, **2** (2017), 188–202. https://doi.org/10.1016/j.idm.2017.04.002

20. H. McCallum, N. Barlow, J. Hone, How should pathogen transmission be modelled?, *Trends Ecol. Evol.*, **16** (2001), 295–300. https://doi.org/10.1016/S0169-5347(01)02144-9

21. K. S. Kim, K. Ejima, Y. Ito, S. Iwanami, H. Ohashi, Y. Koizumi, et al., Modelling SARS-CoV-2 dynamics: Implications for therapy, *PLoS Biol.*, **19** (2021), e3001128. https://doi.org/10.1371/journal.pbio.3001128

22. M. Menale, R. Travaglini, A nonconservative kinetic model under the action of an external force field for modeling the medical treatment of autoimmune response, *Commun. Nonlinear Sci. Numer. Simul.*, **137** (2024), 108126. https://doi.org/10.1016/j.cnsns.2024.108126

23. L. Cuesta-Herrera, L. Pastenes, F. Cordova-Lepe, A. D. Arencibia, H. Torres-Mantilla, J. P. Gutierrez-Jara, Analysis of SEIR-type models used at the beginning of COVID-19 pandemic reported in high-impact journals, *Medwave*, **22** (2022), 2552. https://doi.org/10.5867/medwave.2022.08.2552

24. J. E. Andrades-Grassi, L. Cuesta-Herrera, G. Bianchi-Pérez, H. C. Grassi, J. Y. López-Hernández, H. Torres-Mantilla, Spatial analysis of risk of morbidity and mortality by COVID-19 in Europe and the Mediterranean in the year 2020, *Cuadernos Geográficos*, **60** (2021), 279–294. https://doi.org/10.30827/cuadgeo.v60i1.15492

25. K. S. Kim, K. Ejima, S. Iwanami, Y. Fujita, H. Ohashi, Y. Koizumi, et al., A quantitative model used to compare within-host SARS-CoV-2, MERS-CoV, and SARS-CoV dynamics provides insights into the pathogenesis and treatment of SARS-CoV-2, *PLoS Biol.*, **19** (2021), e3001128. https://doi.org/10.1371/journal.pbio.3001128

26. P. Abuin, A. Anderson, A. Ferramosca, E. A. Hernandez-Vargas, A. H. Gonzalez, Characterization of SARS-CoV-2 dynamics in the host, *Ann. Rev. Control*, **50** (2020), 457–468. https://doi.org/10.1016/j.arcontrol.2020.09.008
27. E. A. Hernandez-Vargas, *Modeling and Control of Infectious Diseases in the Host: With MATLAB and R*, Academic Press, 2019.
28. M. A. Nowak, C. R. M. Bangham, Population dynamics of immune responses to persistent viruses, *Science*, **272** (1996), 74–79. https://doi.org/10.1126/science.272.5258.74
29. T. W. Alleman, J. Vergeynst, L. De Visscher, M. Rollier, E. Torfs, I. Nopens, et al., Assessing the effects of non-pharmaceutical interventions on SARS-CoV-2 transmission in Belgium by means of an extended SEIQRD model and public mobility data, *Epidemics*, **37** (2021), 100505. https://doi.org/10.1016/j.epidem.2021.100505
30. B. C. K. Choi, A. W. P. Pak, A simple approximate mathematical model to predict the number of severe acute respiratory syndrome cases and deaths, *J. Epidemiol. Commun. Health*, **57** (2003), 831–835. https://doi.org/10.1136/jech.57.10.831
31. M. Lipsitch, T. Cohen, B. Cooper, J. M. Robins, S. Ma, L. James, et al., Transmission Dynamics and Control of Severe Acute Respiratory Syndrome, *Science*, **300** (2003), 1966–1970. https://doi.org/10.1126/science.1086616
32. J. O. Lloyd-Smith, A. P. Galvani, W. M. Getz, Curtailing transmission of severe acute respiratory syndrome within a community and its hospital, *Proc. R. Soc. London Ser. B Biol. Sci.*, **270** (2003), 1979–1989. https://doi.org/10.1098/rspb.2003.2481
33. S. Riley, C. Fraser, C. A. Donnelly, A. C. Ghani, L. J. Abu-Raddad, A. J. Hedley, et al., Transmission dynamics of the etiological agent of sars in hong kong: Impact of public health interventions, *Science*, **300** (2003), 1961–1966. https://doi.org/10.1126/science.1086478
34. R. Della Marca, N. Loy, A. Tosin, An SIR model with viral load-dependent transmission, *J. Math.Biol.*, **86** (2023), 61. https://doi.org/10.1007/s00285-023-01901-z
35. C. E. Mills, J. M. Robins, M. Lipsitch, Transmissibility of 1918 pandemic influenza, *Nature*, **432** (2004), 904–906. https://doi.org/10.1038/nature03063
36. A. Stegeman, A. Bouma, A. R. W. Elbers, M. C. M. de Jong, G. Nodelijk, F. de Klerk, et al., Avian influenza A virus (H7N7) epidemic in The Netherlands in 2003: Course of the epidemic and effectiveness of control measures, *J. Infect. Dis.*, **190** (2004), 2088–2095. https://doi.org/10.1086/425583
37. K. Y. Ng, M. M. Gui, COVID-19: Development of a robust mathematical model and simulation package with consideration for ageing population and time delay for control action and resusceptibility, *Phys. D Nonlinear Phenom.*, **411** (2020), 132599. https://doi.org/10.1016/j.physd.2020.132599
38. M. J. Wonham, T. de-Camino-Beck, M. A. Lewis, An epidemiological model for West Nile virus: Invasion analysis and control applications, *Proc. Roy. Soc. London Ser. B Biol. Sci.*, **271** (2004), 501–507. https://doi.org/10.1098/rspb.2003.2608

39. T. J. Sego, J. O. Aponte-Serrano, J. Ferrari Gianlupi, S. R. Heaps, K. Breithaupt, L. Brusch, et al., A modular framework for multiscale, multicellular, spatiotemporal modeling of acute primary viral infection and immune response in epithelial tissues and its application to drug therapy timing and effectiveness, *PLoS Comput. Biol.*, **16** (2020), e1008451. https://doi.org/10.1371/journal.pcbi.1008451
40. J. A. Owen, J. Punt, S. A. Stranford, *Kuby Immunol*, WH Freeman New York, NY, USA, 2013.
41. A. K. Abbas, A. H. Lichtman, S. Pillai, *Cellular and Molecular Immunology*, 10th Edition, Elsevier Health Sciences, 2014.
42. L. Perko, *Differential Equations and Dynamical Systems*, Springer, New York, 2013. https://doi.org/10.1007/978-1-4613-0003-8
43. P. van den Driessche, J. Watmough, Reproduction numbers and sub-threshold endemic equilibria for compartmental models of disease transmission, *Math. Biosci.*, **180** (2002), 29–48. https://doi.org/10.1016/S0025-5564(02)00108-6
44. K. A. Walsh, K. Jordan, B. Clyne, D. Rohde, L. Drummond, P. Byrne, et al., SARS-CoV-2 detection, viral load and infectivity over the course of an infection, *J. Infect.*, **81** (2020), 357–371. https://doi.org/10.1016/j.jinf.2020.06.067
45. S. Lee, T. Kim, E. Lee, C. Lee, H. Kim, H. Rhee, et al., Clinical course and molecular viral shedding among asymptomatic and symptomatic patients with SARS-CoV-2 infection in a community treatment center in the Republic of Korea, *JAMA Int. Med.*, **180** (2020), 1447–1452. https://doi.org/10.1001/jamainternmed.2020.3862
46. Y. Liu, L. Yan, L. Wan, T. Xiang, A. Le, J. Liu, et al., Viral dynamics in mild and severe cases of COVID-19, *Lancet Infect. Dis.*, **20** (2020), 656–657. https://doi.org/10.1016/S1473-3099(20)30232-2
47. C. Zhou, T. Zhang, H. Ren, S. Sun, X. Yu, J. Sheng, et al., Impact of age on duration of viral RNA shedding in patients with COVID-19, *Aging*, **12** (2020), 22399. https://doi.org/10.18632/aging.104114
48. A. Amoddeo, A mathematical model and numerical simulation for SARS-CoV-2 dynamics, *Sci. Rep.*, **13** (2023), 4575. https://doi.org/10.1038/s41598-023-31733-2
49. H. Laferl, H. Kelani, T. Seitz, B. Holzer, I. Zimpernik, A. Steinrigl, et al., An approach to lifting self-isolation for health care workers with prolonged shedding of SARS-CoV-2 RNA, *Infection*, **49** (2021), 95–101. https://doi.org/10.1007/s15010-020-01530-4
50. A. Singanayagam, M. Patel, A. Charlett, J. L. Bernal, V. Saliba, J. Ellis, et al., Duration of infectiousness and correlation with RT-PCR cycle threshold values in cases of COVID-19, England, January to May 2020, *Eurosurveillance*, **25** (2020), 2001483. https://doi.org/10.2807/1560-7917.ES.2020.25.32.2001483
51. Y. Sohn, S. J. Jeong, W. S. Chung, J. H. Hyun, Y. J. Baek, Y. Cho, et al., Assessing viral shedding and infectivity of asymptomatic or mildly symptomatic patients with COVID-19 in a later phase, *J. Clin. Med.*, **9** (2020), 2924. https://doi.org/10.3390/jcm9092924

52. K. Ejima, K. S. Kim, C. Ludema, A. I. Bento, S. Iwanami, Y. Fujita, et al., Estimation of the incubation period of COVID-19 using viral load data, *Epidemics*, **35** (2021), 100454. https://doi.org/10.1016/j.epidem.2021.100454

53. J. D. Challenger, C. Y. Foo, Y. Wu, M. M. Marjaneh, F. Liew, R. S. Thwaites, et al., Modelling upper respiratory viral load dynamics of SARS-CoV-2, *BMC Med.*, **20** (2022). https://doi.org/10.1186/s12916-021-02220-0

54. S. Iwami, K. Sato, R. J. De Boer, K. Aihara, T. Miura, Y. Koyanagi, Identifying viral parameters from in vitro cell cultures, *Front. Microbiol.*, **3** (2012), 319. https://doi.org/10.3389/fmicb.2012.00319

55. A. Bondesan, A. Piralla, E. Ballante, A. M. G. Pitrolo, S. Figini, F. Baldanti, et al., Predictability of viral load dynamics in the early phases of SARS-CoV-2 through a model-based approach, *Math. Biosci. Eng.*, **22** (2025), 725–743. https://doi.org/10.3934/mbe.2025027

56. R. Wölfel, V. M. Corman, W. Guggemos, M. Seilmaier, S. Zange, M. A. Müller, et al., Virological assessment of hospitalized patients with COVID-2019, *Nature*, **581** (2020), 465–469. https://doi.org/10.1038/s41586-020-2196-x

57. M. Sadria, A. T. Layton, Use of angiotensin-converting enzyme inhibitors and angiotensin ii receptor blockers during the Covid-19 pandemic: A modeling analysis, *PLoS Comput. Biol.*, **16** (2020), e1008235. https://doi.org/10.1371/journal.pcbi.1008235

AIMS Press